

Properties of Diazocarbene [CNN] and the Diazomethyl Radical [HCNN] via Ion Chemistry and Spectroscopy

Eileen P. Clifford,[§] Paul G. Wenthold,[¶] W. Carl Lineberger,^{*,¶} George A. Petersson,^{*,†} Katherine M. Broadus,[‡] Steven R. Kass,^{*,‡} Shuji Kato,[§] Charles H. DePuy,^{*,§} Veronica M. Bierbaum,^{*,§} and G. Barney Ellison^{*,§}

Department of Chemistry & Biochemistry, University of Colorado, Boulder, Colorado 80309-0215, JILA and the Department of Chemistry & Biochemistry, University of Colorado, Boulder, Colorado 80309-0440, Hall Atwater Laboratories of Chemistry, Wesleyan University, Middletown, Connecticut 06459-0180, and Department of Chemistry, University of Minnesota, Minneapolis, Minnesota 55455

Received: November 20, 1997; In Final Form: February 20, 1998

We have used negative ion photoelectron spectroscopy to measure the electron affinities of diazocarbene and the diazomethyl radical: $EA(\tilde{X}^3\Sigma^- \text{CNN}) = 1.771 \pm 0.010$ eV, $EA(\tilde{X}^2A'' \text{HCNN}) = 1.685 \pm 0.006$ eV, and $EA(\tilde{X}^2A'' \text{DCNN}) = 1.678 \pm 0.006$ eV. Our experimental findings are accurately reproduced by complete basis set (CBS) ab initio electronic structure calculations: $EA(\tilde{X}^3\Sigma^- \text{CNN}) = 1.83 \pm 0.03$ eV, $EA(\tilde{X}^2A'' \text{HCNN}) = 1.69 \pm 0.03$ eV. We make use of the electron affinities of CNN and HCNN, together with the gas phase acidity of diazomethane, $\Delta_{\text{acid}}H_{298}(\text{HCHN}_2) = 372.2 \pm 2.1$ kcal mol⁻¹ (CBS calculated value = 373.4 ± 0.7), to find the bond enthalpies of H₂CNN. We find $DH_{298}(\text{H}-\text{CHN}_2)$ equal to 97 ± 2 kcal mol⁻¹, which closely agrees with the CBS-QCI/APNO-calculated value [$DH_{298}(\text{H}-\text{CHN}_2) = 98.5 \pm 0.7$ kcal mol⁻¹]. From proton transfer experiments in a Fourier transform mass spectrometer and a tandem flowing afterglow-selected ion flow tube (FA-SIFT), we find $\Delta_{\text{acid}}H_{298}(\text{HCNN}) = 352 \pm 4$ kcal mol⁻¹ in agreement with the CBS-QCI/APNO-calculated value of 351.8 ± 0.7 kcal mol⁻¹. Use of the experimental electron affinity, $EA(\text{CNN})$, leads to the CH bond enthalpy of the cyanoamino radical, $DH_{298}(\text{H}-\text{CNN}) = 79 \pm 4$ kcal mol⁻¹ which is in excellent agreement with the CBS-QCI/APNO-calculated value: $DH_{298}(\text{H}-\text{CNN}) = 78.7 \pm 0.7$ kcal mol⁻¹. If we adopt the CBS-QCI/APNO value for $\Delta_f H_{298}(\text{CH}_2\text{N}_2)$ [64.1 ± 0.7 kcal mol⁻¹] as our reference, we obtain $\Delta_f H_{298}(\text{HCN}_2) = 110 \pm 2$ kcal mol⁻¹ and $\Delta_f H_{298}(\text{CN}_2) = 136 \pm 5$ kcal mol⁻¹, which are again in agreement with the CBS-QCI/APNO values: $\Delta_f H_{298}(\text{HCN}_2) = 110.5 \pm 0.7$ kcal mol⁻¹ and $\Delta_f H_{298}(\text{CN}_2) = 138.4 \pm 0.7$ kcal mol⁻¹. We recommend revised experimental values for $\Delta_f H_0(\text{HCN}) = 30.9 \pm 0.7$ kcal mol⁻¹ and $\Delta_f H_{298}(\text{HCN}) = 30.8 \pm 0.7$ kcal mol⁻¹ and find that the reaction $\text{CH}(^2\Pi) + \text{N}_2 \rightarrow \text{HCN} + \text{N}(^4\text{S})$ to be slightly endothermic, $\Delta_{\text{rxn}}H_0 = 1.6 \pm 0.7$ kcal mol⁻¹.

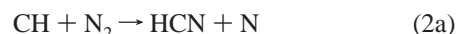
I. Introduction

In an internal combustion engine, air is the source of most of the N atoms which produce nitric oxide. Three mechanisms are proposed¹ for the production of NO and these are designated as “fuel NO”, “thermal NO”, and “prompt NO.” Nitrogen-containing fuels (“fuel NO”) will have obvious routes to produce NO_x but most fuels are hydrocarbons. It has been known¹ for some time that “thermal” NO is generated in the post-combustion region by the Zeldovich mechanism involving O atoms and N₂.

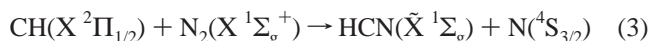


In most combustion processes, hydrocarbons are degraded to produce radicals such as C, CH, and CH₂. The “prompt” formation of NO at the flame front is now recognized to involve

chemistry of the CH radical via the Fenimore mechanism:^{2,3}



The reaction of the CH radical with N₂ in (2a) provides an interesting problem because spin is not conserved. This reaction is written explicitly in (3)



The organic radical CH is known to cleave N₂ to generate HCN and N atoms, and it is conjectured that the adduct HCNN is an important intermediate in this process. The diazomethyl (HCNN) and diazocarbene (CNN) radicals are important combustion species because they provide low energy paths to cleave N₂ to produce N atoms which are then rapidly oxidized to nitric oxide.⁴ Thus the reaction of CH with N₂ to produce N

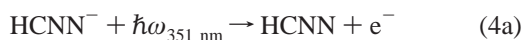
[§] Department of Chemistry & Biochemistry, University of Colorado.
[¶] JILA and the Department of Chemistry & Biochemistry, University of Colorado.

[†] Wesleyan University.

[‡] University of Minnesota.

atoms connects internal combustion engines with NO production. Nitric oxide emissions are the major factor driving urban air pollution and automobiles are the major source of NO in cities.

In this paper we will use negative ion photoelectron spectroscopy to characterize both the diazomethyl radical and diazocarbene.



Our study of the spectroscopy of these radicals enables the extraction of a number of thermodynamic constants. We will use our results to establish the thermochemistry of HCNN and CNN. Finally, with the experimental characterization of the HCNN and CNN species, we will make some observations about the mechanism of (3) at the conclusion of the paper.

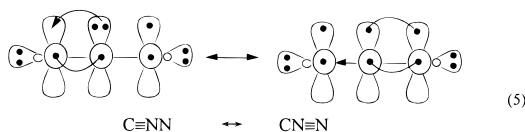
How can we describe the electronic structure of CN_2 and HCN_2 and what are the adducts of C or CH with N_2 ? In this paper we will study only the "linear" species HCNN and CNN. The rings, the diazirinyl radical



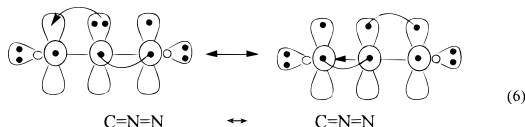
and the diazirinylcarbene



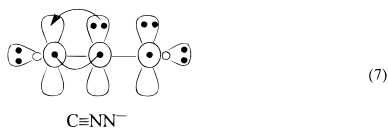
will be addressed in future studies. The combination of C (^3P) with N_2 ($^1\Sigma_g^+$) leads to CNN which can be written^{5,6} as a dative or coordinate structure, $\text{CNN } \tilde{\text{X}} (^3\Sigma^-)$:



Expression 5 for CNN can also be coupled as a singlet: $^1\Delta$ or $^1\Sigma^+$. The formulas for the singlets are written in such a way as to minimize exchange coupling of the radical pair of electrons, $K_{\pi\pi}$, so one might write the $\tilde{\text{a}} ^1\Delta$ state as:



Starting with either (5) or (6), one would predict that the CNN^- ion is $\tilde{\text{X}} ^2\Pi$.

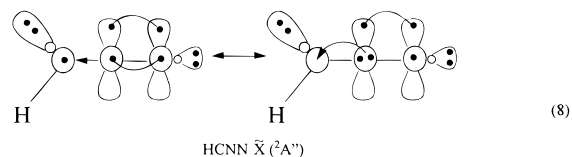


The earliest experimental identification of the CNN carbene consisted of weak UV signals observed following irradiation^{7,8} of matrix isolated H_2CN_2 . Diazocarbene has also been prepared from the photodecomposition of NCN_3 in a cryogenic matrix and studied by EPR spectroscopy.⁹ Analysis of the magnetic resonance spectrum led to the conclusion that the ground state of CNN is $\tilde{\text{X}} ^3\Sigma^-$. The infrared absorption spectrum of CNN

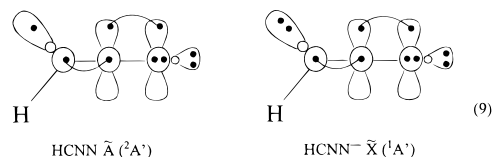
$\tilde{\text{X}} ^3\Sigma^-$ was studied¹⁰ in Ar and N_2 matrices at 14 K. Irradiation of NCN_3 at 2100–2800 Å was used to produce CNN. The three fundamentals were assigned as ν_1 [symmetric stretch (sym st)] = 1241 cm^{-1} , ν_2 (bend) = 393 cm^{-1} , ν_3 [asymmetric stretch (asym st)] = 2847 cm^{-1} . UV bands of CNN were observed at 4189 Å (23872 cm^{-1}) and 3964 Å (25227 cm^{-1}). Irradiation of CH_4 with Ly α (1216 Å) generated C atoms which combined with N_2 to produce the CNN carbene in a nitrogen matrix.¹¹ LIF studies of $\tilde{\text{X}} ^3\Sigma^- \leftarrow \tilde{\text{A}} ^3\Pi$ led to the assignment $T_0(\text{CNN}) = 23597 \text{ cm}^{-1}$, and these spectra revealed constants for $\tilde{\text{A}} ^3\Pi$ (CNN): $\nu_1 = 1807$, $\nu_2 = 525$, $\nu_3 = 1322 \text{ cm}^{-1}$. The spin-orbit splitting was observed in $\tilde{\text{A}} ^3\Pi_{2,1,0}(\text{CNN})$ and is $|A| = 9 \text{ cm}^{-1}$, while the Renner–Teller parameter for the $^3\Pi$ state is $\epsilon = -0.07$. An early ab initio electronic structure calculation¹² of the geometry and harmonic frequencies of diazocarbene suggested that the asymmetric stretch of $\tilde{\text{X}} ^3\Sigma^-$ was misassigned and that the vibrational frequencies should be reconsidered. Recently,¹³ FT-LIF studies of $\tilde{\text{X}} ^3\Sigma^- - \tilde{\text{A}} ^3\Pi$ were reported, and the asymmetric stretch (ν_3) was reassigned as 1419 cm^{-1} in accordance with the ab initio predictions. These LIF studies suggested that diazocarbene has an unusual electronic structure such that the infrared intensity of ν_3 is "accidentally" zero. The previous value of 2847 cm^{-1} is actually the overtone $3\nu_2$.

Gas-phase reaction¹⁴ of C atoms (ablated by a laser) with N_2 produced the CNN radical. The subsequent LIF studies of $\tilde{\text{X}} ^3\Sigma^- - \tilde{\text{A}} ^3\Pi$ found $T_0(\tilde{\text{A}} ^3\Pi) = 23850 \text{ cm}^{-1}$. These LIF studies reported the rotational constants for both states: $\tilde{\text{X}} ^3\Sigma^-$ (CNN) $B_0 = 0.4136 \pm 0.0100 \text{ cm}^{-1}$ and $\tilde{\text{A}} ^3\Pi$ (CNN) $B_0 = 0.4250 \pm 0.010 \text{ cm}^{-1}$. Table 1 summarizes the molecular constants^{13–15} of diazocarbene.

The HCNN molecule can be assembled¹⁶ by addition of CH ($^2\Pi$) to N_2 or by the combination of a hydrogen atom with the dative structure shown for CNN $\tilde{\text{X}} (^3\Sigma^-)$ above in (5). The resulting $\tilde{\text{X}} (^2\text{A}'')$ of HCNN can be written as a resonance formula:



Using $\text{HCNN } \tilde{\text{X}} (^2\text{A}'')$, one would write the corresponding anion as HCNN^- , $\tilde{\text{X}} (^1\text{A}')$. Similarly one expects that there will be a low-lying excited state of diazomethyl radical, $\text{HCNN } \tilde{\text{A}} (^2\text{A}')$. These species are shown in (9).



As the diazomethyl radical becomes linear, the $\tilde{\text{X}} (^2\text{A}'')$ and $\tilde{\text{A}} (^2\text{A}')$ states will collapse together as a degenerate Renner–Teller pair, $^2\Pi$ HCNN.

Very little is known experimentally about the HCNN molecule. Mercury lamp irradiation of matrix-isolated H_2CN_2 produced the diazomethyl radical.¹⁷ A few of the infrared-active fundamentals of HCNN were observed and these are listed in Table 1.

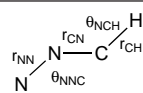
The diazomethyl radical and diazocarbene have been the subject of several ab initio electronic structure calculations, summarized in Table 2. Early studies¹² of CNN suggested that the computed properties of this carbene varied wildly depending

TABLE 1: Molecular Constants

Diazocarbene, CNN						
State	B_0/cm^{-1}	T_0/cm^{-1}	ν_1/cm^{-1}	ν_2	ν_3	ref
$\tilde{X}^3\Sigma^-$ (Ar matrix)			1241	393	2847	10, 11
$\tilde{X}^3\Sigma^-$ (Ar matrix)	0.4136 ± 0.0100		1235	396	1419	13, 14
$\tilde{A}^3\Pi$ (Ar matrix)		23 597	1325	525	1807	7, 8, 11, 13
$\tilde{A}^3\Pi$ (gas phase)	0.4250 ± 0.0100	23 850				14
$\tilde{B}^3\Sigma^-$ (Ar matrix)		$\leq 39\ 950$				15
$\tilde{C}^3\Pi$ (Ar matrix)		48 540				15
Diazomethyl Radical, HCNN						
State						ref
\tilde{X}	H—CNN stretch		3233 (Ar matrix)			15, 17
	HC—N—N asym stretch		3229 (N ₂ matrix)			
			1787 (Ar matrix)			
			1784 (Kr matrix)			
			1800 (N ₂ matrix)			
	H—CNN bend		861 (Ar matrix)			
			860 (Kr matrix)			
\tilde{A}	DC—N—N asym stretch		871 (N ₂ matrix)			15
	D—CNN bend		1771 (Ar matrix)			
	HCNN		725 (Ar matrix)			
			$T_0 = 30\ 500\ \text{cm}^{-1}$			

TABLE 2: Ab Initio Electronic Structure Calculations for CNN $\tilde{X}^3\Sigma^-$ /HCNN \tilde{X}^2A''

CNN $\tilde{X}^3\Sigma^-$							
calculation	harmonic frequencies, ω/cm^{-1} [infrared intensities, A/km mol^{-1}]						ref
	energy/au	$r_{\text{CN}}/\text{Å}$	$r_{\text{NC}}/\text{Å}$	ω_1 (symmetric stretch)	ω_2 (bend)	ω_3 (asymmetric stretch)	
ROHF/DZ	-146.59094	1.175	1.357				68
ROHF/DZ+P	-146.68096	1.159	1.339				
ROHF/DZ+P	-146.66081	1.169	1.307	2295[385]	320[1]	1091[47]	12
ROHF/TZ+P	-146.67237	1.155	1.294	2266[354]	299[2]	1063[44]	
CISD/DZ+P	-147.01025	1.203	1.939	1939[359]	359[3]	1041[22]	
CASSCF/DZ+P	-146.78575	1.241	1.223	1461[15]	na ^a	1177[0.3]	
UHF/DZ+P	-146.68336	1.198	1.205	1797[na]	386[na]	1169[na]	
B3LYP-ROKS/DZP		1.271	1.225	1226[14]	402[9]	1411[1]	69
B3LYP-ROKS/DZP		1.271	1.225	1226[14]	402[9]	1411[1]	
B3LYP-ROKS/TZ2P		1.254	1.204	1235[17]	361[7]	1401[3]	
B3LYP-ROKS/TZ2P+f		1.252	1.204	1241[18]	393[7]	1429[3]	
B3LYP-UKS/DZP		1.273	1.226	1220[11]	398[9]	1455[2]	
B3LYP-UKS/TZ2P		1.254	1.205	1229[14]	357[8]	1444[3]	
B3LYP-UKS/TZ2P+f		1.253	1.205	1235[14]	389[8]	1469[3]	
UHF-QCISD/6-31G*		1.231	1.237	1205	na	1537	70

HCNN \tilde{X}^2A'' 

calculation	energy/au	$r_{\text{NN}}/\text{Å}$	$r_{\text{NC}}/\text{Å}$	$r_{\text{CH}}/\text{Å}$	θ_{NNC}	θ_{NCH}	ref
ROHF/DZ	-146.59094	1.175	1.357				68
ROHF/DZ+P	-146.68096	1.159	1.339				68
SOCI/TZ2P	-147.71492	1.143	1.340	1.082		110.88	62
CASSCF/TZ2P	-147.45136	1.1527	1.3110	1.0755	168.03	113.24	64

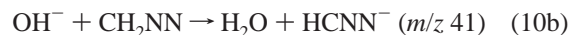
^a na = not available.

upon the size of the basis set and nature of the Hamiltonian [as the diagram in (5) suggests]. These calculations correctly assigned the asymmetric stretch of CNN as $\nu_3 = 1419\ \text{cm}^{-1}$ and $\neq 2847\ \text{cm}^{-1}$.

II. Experimental Procedures

A. Negative Ion Photoelectron Spectroscopy. The photoelectron spectra were collected on a spectrometer that has been described elsewhere.^{18,19} We have used oxide ion chemistry^{20,21} to generate CNN⁻ from diazomethane; CH₂NN and CD₂NN were synthesized by standard methods²² and purified by several freeze-pump-thaw cycles on a vacuum line. The chemistry²¹

used to produce the target ions is



The two ions at m/z 40 and 41 were separated by a Wien velocity filter and were photodetached by a CW Ar III ion laser that provides 50–100 W of 351.1 nm light in the circulating build-up cavity. The photodetached electrons are focused and pass through a hemispherical energy analyzer, with an instrumental resolution (fwhm) of 6–10 meV. In order to reduce rotational broadening in the photodetachment spectra, we bathe part of

the flow tube with liquid N₂. The vibrational and rotational temperatures of the ions are roughly 200 K.

The photoelectron spectra are calibrated²³ with respect to O⁻ and transformed to the center of mass (cm) frame by a standard expression²⁴ where E is the center of mass (cm) kinetic energy (eV) of an electron detached from an ion of mass M (amu) which is passed by the energy analyzer when the slit voltage is V . The beam energy is W , m_e is the mass of an electron, and γ is the dimensionless scale compression factor (typically 1.000 ± 0.006):

$$E = E_{\text{cal}} + \gamma(V - V_{\text{cal}}) + m_e W \left(\frac{1}{M_{\text{cal}}} - \frac{1}{M} \right)$$

B. Negative Ion Mass Spectroscopy. *FTMS: Experimental.* The gas phase acidities of CH₂N₂ and HCN₂ were measured in a Fourier transform mass spectrometer (FTMS). A dual cell model 2001 Finnigan FTMS equipped with a 3.0 T superconducting magnet was used to measure the proton affinities of CHN₂⁻ and CNN⁻. The first of these values was determined by measuring the forward (k_{11}) and reverse (k_{-11}) rate constants, and thus the equilibrium constant ($k_{11}/k_{-11} = K_{\text{equi}}$), for the acid–base reactions with acetonitrile and its conjugate base (11).



A decalin solution of diazomethane was synthesized from *N*-nitroso-*N*-methyl urea and 50% wt KOH as previously described.²² Fluoride ion was formed by electron-impact ionization (6 eV) of carbon tetrafluoride, which was pulsed into one of the cells at a pressure of 1×10^{-6} Torr. This ion was allowed to react for ca. 2.0 s with a static pressure of diazomethane (ca. 6×10^{-8} Torr), which was introduced into the cell via a slow leak valve, to afford diazomethyl anion (CHN₂⁻). Diazomethyl anion was subsequently isolated by applying the appropriate radio frequencies (SWIFT)²⁵ to eject F⁻, CF₃⁻, and any other ions present in the cell. The CHN₂⁻ anion was then transferred to the second cell and argon was pulsed (2×10^{-6} Torr) into the cell in order to thermalize the ions. A static pressure of CH₃CN (which was varied from ca. 5×10^{-8} to 1.0×10^{-7} Torr) also was present in order to effect the proton transfer reaction. The reverse reaction (–11) was examined by deprotonating acetonitrile with fluoride and then reacting CH₂CN⁻ with diazomethane.

Reaction rates for (11) were determined by monitoring the disappearance of the reactant anion after allowing a 600 ms interval for vibrational cooling with the added argon. All of the reactions were followed over a 3–5 s time period (about 2 half-lives) under pseudo-first-order conditions. The bimolecular rate constant (k^{II}) was obtained using the following equation:

$$k^{\text{II}} = \frac{k_{\text{obs}} R_x T}{9.66 \times 10^{18} [P]} \quad (12)$$

where k_{obs} = the slope of $\ln[\text{anion}]$ vs time (in seconds), R_x = the pressure gauge correction for the neutral²⁶ (a function of polarizability²⁷), $T = 300$ K, and P = the pressure of the neutral compound (Torr).

The atomic oxygen ion (O⁻) was generated by electron-impact ionization (1.6 eV) of a pulse of nitrous oxide (ca. 1×10^{-6} Torr). This ion was allowed to react for 2.0 s with a static pressure of diazomethane (ca. 6×10^{-8} Torr) to give both CHN₂⁻ and CNN⁻ in about a 1:2 ratio. The latter species was isolated in one cell (SWIFT)²⁵ and then transferred to the other where the ions were thermally equilibrated by collisions with

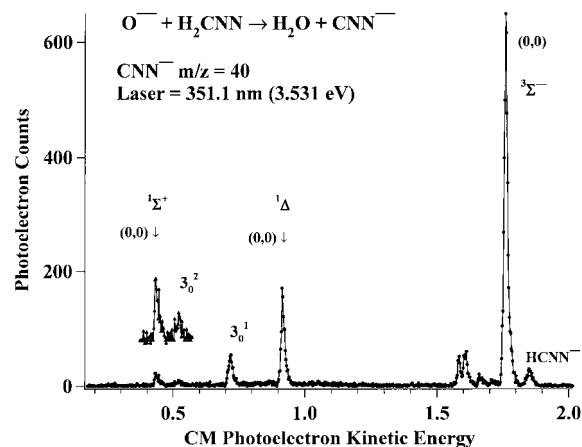


Figure 1. Negative ion photoelectron spectrum of the CNN⁻ ion: the (0,0) feature occurs at an electron kinetic energy of 1.761 ± 0.010 eV.

argon at pressures in excess of 10^{-6} Torr. The CNN⁻ ion was then added to different reference acids at static pressures of roughly 1×10^{-7} Torr. To ensure that the observed conjugate bases (A⁻) were not the result of hot ions, the initial product ions were ejected from the cell and proton transfer was recorded as positive only if A⁻ grew back in with time. In one instance (the reaction with CH₃CH₂SH), diazomethane was used as the collision gas since it should be a more efficient quencher for CNN⁻. No difference (compared to Ar) was noted.

FA-SIFT: Experimental. A tandem flowing afterglow-selected ion flow tube was employed to bracket the gas phase basicity of CNN⁻. The instrument has been described in detail previously.²⁸ The O⁻ ion is generated in the source flow tube by electron impact on traces of nitrous oxide in the helium buffer gas (0.3 Torr). Diazomethane is then added from a solution in decalin, and CNN⁻ is formed by a rapid dehydrogenation reaction. The ions are extracted from the source flow tube, focused with a series of lenses, and the CNN⁻ ions are mass selected by a quadrupole mass filter. The helium and neutral precursors are removed by pumping and the mass selected ions are refocused and injected through a Venturi inlet into the reaction flow tube. The ions are entrained in a fast flow of helium buffer gas ($v = 80$ m/s and $P = 0.5$ Torr) and allowed to undergo thousands of collisions with helium before entering the reaction region. The bracketing acids [CH₃SH, C₂H₅SH, (CH₃)₂CSH, or CH₃CO₂H] are introduced through a manifold of inlets, and the reactant and product ions are monitored with a detection quadrupole mass filter coupled with an electron multiplier. The flow rates of the neutral reagents are measured by monitoring the pressure increase with time in a calibrated volume system. Bimolecular rate constants are determined from the slope of the semi-logarithmic decay of the reactant ion as a function of reaction distance, the measured reactant and helium flow rates, the pressure of helium, and the temperature (300 K). Small corrections were made to the product distributions to account for the reactions of HCNN⁻ ions which were present in trace amounts ($\approx 1\%$ of CNN⁻).

III. Results

A. Photoelectron Spectroscopy. Figure 1 presents the photoelectron spectrum of the CNN⁻ ion. Because of imperfect mass-resolution, this spectrum is slightly contaminated with a peak due to the HCNN⁻ ion. There are three sets of transitions in the CNN⁻ spectrum. The peaks with the highest kinetic energy (≈ 1.75 eV) correspond to detachment from the $\tilde{X}^2\Pi$ CNN⁻ ion to the $\tilde{X}^3\Sigma^-$ ground state of CNN. The features at

TABLE 3: Photoelectron Bands^a

species	Angular Distributions fit to $I(\theta) = \bar{\sigma}/4\pi[1 + \beta(E)P_2(\cos\theta)]$			
	cm kinetic energy/eV	vibrational splitting/cm ⁻¹	electronic splitting/eV	anisotropy $\beta(E)$
CNN ← CNN ⁻ ³ Σ ⁻				
(0,0)	1.761 ± 0.010			
2 ₀ ¹	1.712 ± 0.011	392 ± 120		
2 ₀ ²	1.665 ± 0.011	771 ± 120		
1 ₀ ¹	1.608 ± 0.011	1231 ± 120		
3 ₀ ¹	1.584 ± 0.011	1424 ± 120		
β(³ Σ ⁻)				-0.91 ± 0.15
¹ Δ				
(0,0)	0.915 ± 0.010		0.846 ± 0.014	
3 ₀ ¹	0.717 ± 0.011	1597 ± 120		
3 ₀ ²	0.519 ± 0.011	3194 ± 120		
β(¹ Δ)				-0.43 ± 0.15
¹ Σ ⁺				
(0,0)	0.436 ± 0.011		1.325 ± 0.015	
HCNN ← HCNN ⁻ ² A''				
(0,0)	1.847 ± 0.006			
5 ₀ ¹	1.787 ± 0.006	484 ± 70		
2 ₀ ¹	1.626 ± 0.007	1782 ± 77		
2 ₀ ¹ 5 ₀ ¹	1.567 ± 0.008	2258 ± 81		
β(² A'')				-0.84 ± 0.15
² A'				
(0,0)	≅ 1.172 ± 0.010	0.522 ± 0.012 ≤ T ₀ ≤ 0.675 ± 0.012		
β(² A')				0.0 ± 0.15
DCNN ← DCNN ⁻ ² A''				
(0,0)	1.853 ± 0.006			
5 ₀ ¹	1.796 ± 0.006	460 ± 70		
2 ₀ ¹	1.631 ± 0.007	1791 ± 74		
2 ₀ ¹ 5 ₀ ¹	1.578 ± 0.007	2218 ± 78		
² A'				
(0,0)	≅ 1.176 ± 0.010	0.522 ± 0.012 ≤ T ₀ ≤ 0.677 ± 0.012		

^a Final results. The features for CNN are fit to a Gaussian peak shape to within ±0.002 eV and this molecule requires a rotational correction (-0.0004 eV), a CNN⁻ spin-orbit correction (roughly 60 cm⁻¹ or 0.007 eV), and accommodation for the uncertainty in the energy linearity of the analyzer (0.006 eV). After provision for rotational and spin-orbit uncertainties is made, the (0,0) peak is located at cm kinetic energy 1.760 eV. Since the laser energy is 3.531 eV, we find EA($\tilde{X}^3\Sigma^-$ CNN) = 1.771 ± 0.010 eV. The transitions of HCNN are fit to a Gaussian peak shape to within ±0.002 eV, and this molecule requires a rotational correction (-0.0007 eV) and no spin-orbit correction. After provision for this rotational uncertainty is made, the (0,0) peak is located at cm kinetic energy 1.846 ± 0.006 eV. Since the laser energy is 3.531 eV, we find EA(\tilde{X}^2A'' HCNN) = 1.685 ± 0.006 eV and EA(\tilde{X}^2A' DCNN) = 1.678 ± 0.006 eV.

about 0.9 eV are assigned to $\tilde{a}^1\Delta$ CNN, and the weak band at roughly 0.4 eV belongs to the $\tilde{b}^1\Sigma^+$ state of CNN. The positions of these peaks are collected together in Table 3. The (0,0) band occurs at cm kinetic energy 1.761 ± 0.010 eV. Since the laser wavelength is $\lambda_0 = 351.1$ nm (3.531 eV), the uncorrected or "raw" electron affinity is EA(CNN) = 1.770 ± 0.010 eV. There are no prior reports of any singlet states of CNN. We find $T_0(^1\Delta$ CNN) = 0.846 ± 0.014 eV and $T_0(^1\Sigma^+$ CNN) = 1.325 ± 0.015 eV. We assign the fine structure of the ¹Δ CNN state as the ν_3 fundamental (1600 ± 120 cm⁻¹) and the overtone (3₀² = 3195 ± 120 cm⁻¹).

Figure 2 is an expanded trace of the $\tilde{X}^3\Sigma^-$ CNN state. We can use the CNN constants from Table 1 to identify many of the bands. We assign a pair of features to excitation of the symmetric CNN stretch, 1₀¹ (1230 ± 120 cm⁻¹), and the asymmetric stretch, 3₀¹ (1425 ± 120 cm⁻¹). We clearly observe the overtone of the CNN bend as well, 2₀² (770 ± 120 cm⁻¹), and there appears to be a weak feature at a proper energy for the fundamental, 2₀¹ (390 ± 120 cm⁻¹). The weak activity of the bending mode, 2₀¹, is unusual because excitation of a single quantum of a π mode is normally forbidden in a photoelectron spectrum.²⁹ All of these bands appear to be split by roughly

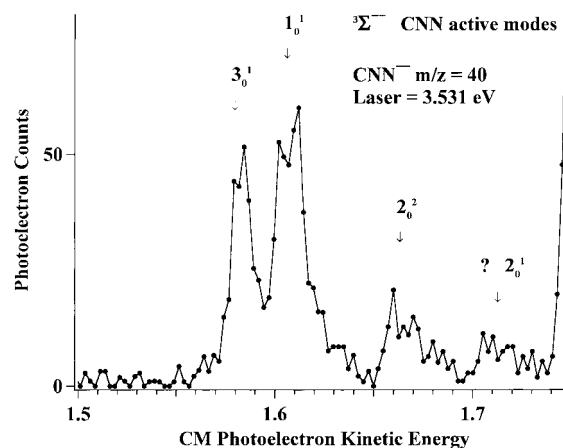


Figure 2. An expanded plot of the vibronic fine structure of the $\tilde{X}^3\Sigma^-$ state of diazocarbene, CNN. We observe excitation of all three vibrational modes of CNN: ν_1 (symmetric CNN stretch, 1199 cm⁻¹), ν_2 (bend, 405 cm⁻¹), and ν_3 (asymmetric CNN stretch, 1420 cm⁻¹). Besides the bending overtone, 2₀² (811 cm⁻¹), we also observe a weak feature at the proper energy for the fundamental, 2₀¹.

40–80 cm⁻¹ and it is likely due to the spin-orbit splitting in the $\tilde{X}^2\Pi$ CNN⁻ ion. The isoelectronic species CNO has been studied³⁰ and for $\tilde{X}^2\Pi_{3/2}$ CNO A'' = -110.5 cm⁻¹.

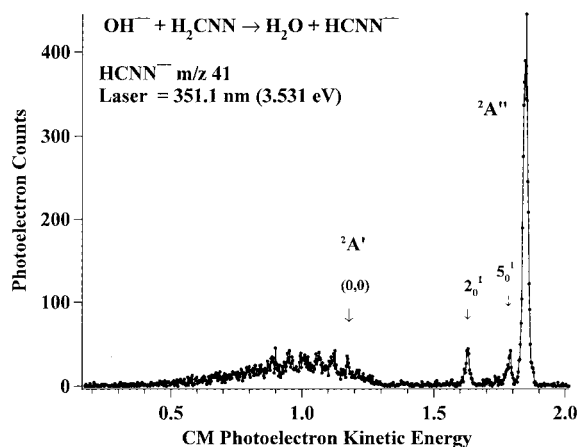


Figure 3. Negative ion photoelectron spectrum of the HCNN^- ion: the (0,0) feature occurs at an electron kinetic energy of 1.852 ± 0.008 eV.

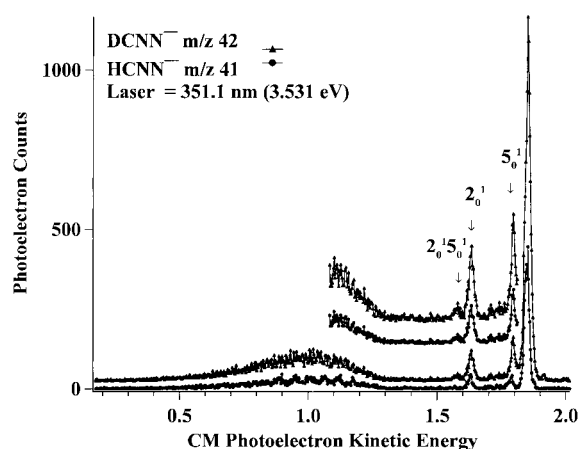


Figure 4. An overlay of the photoelectron spectra of the HCNN^- (●) and DCNN^- (▲) ions. The vibronic features of the $\tilde{X} \ ^2A''$ HCNN state have been enhanced by a factor of two. Excitation of the ν_5 (in-plane N–N–CH bend, 449 cm^{-1}) and ν_2 (asymmetric N–N–CH stretch, 1770 cm^{-1}) modes are marked.

Figure 3 is the photoelectron spectrum of the HCNN^- ion. Two different electronic states are observed which we assign as $\tilde{X} \ ^2A''$ HCNN and $\tilde{A} \ ^2A'$ HCNN. From the Franck–Condon profile of the $\tilde{X} \ ^2A''$ state, we see that the structure of the HCNN^- ion is very close to $\tilde{X} \ ^2A''$ HCNN. In contrast, the geometry of $\tilde{A} \ ^2A'$ HCNN is quite different from that of the HCNN^- anion. In Figure 4, we have plotted an overlay of the photoelectron spectra of HCNN^- and DCNN^- , and it is evident that there is only a small isotope shift. Consequently the active modes are not H-containing fundamentals. This is consistent with the small change in the calculated HCN angle from 109.2° in HCNN^- to 111.0° in $\tilde{X} \ ^2A''$ HCNN. We have relied on the fragmentary HCNN constants (Table 1) and our B3LYP DFT ab initio electronic structure calculations (Table 3) to assign these active modes. The observed low frequency vibration at 485 cm^{-1} must have a' symmetry and consequently cannot be the a'' out-of-plane bending mode. The vibronic features excited in the $\tilde{X} \ ^2A''$ band belong to the in-plane N–N–CH bend, $\nu_5 = 485 \pm 70 \text{ cm}^{-1}$ (5_0^1) and to the asymmetric N–N–CH stretch, $\nu_2 = 1780 \pm 77 \text{ cm}^{-1}$ (2_0^1). Our B3LYP calculations suggest that ν_2 is an intense IR band, and this is certainly the mode observed in the matrix infrared spectrum at 1787 cm^{-1} (Ar matrix).¹⁷ We also observe the combination band, $2_0^1 5_0^1$ (Figure 4). From the spectral origins we compute the “raw” $\text{EA}(\text{HCNN}) = 1.684 \pm 0.006 \text{ eV}$ and the “raw” $\text{EA}(\text{DCNN}) =$

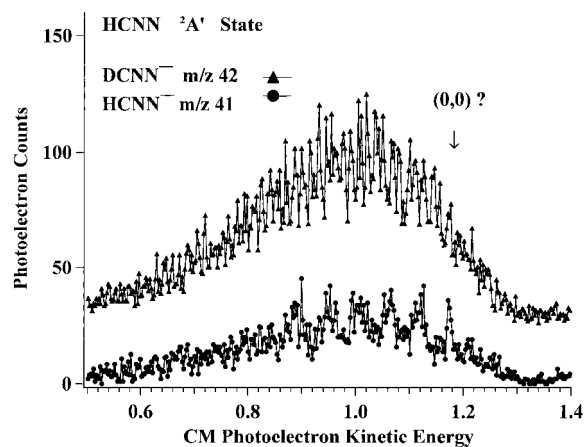
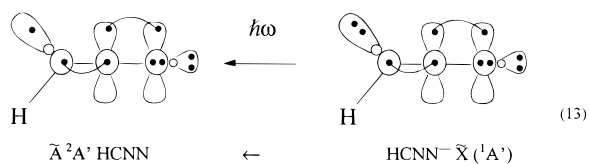


Figure 5. An overlay of the photoelectron spectra of the HCNN^- (●) and DCNN^- (▲) ions in the region of the $\tilde{A} \ ^2A'$ HCNN state. The origin of the $^2A'$ state is $\text{HCNN} (0,0) = 1.172 \pm 0.010 \text{ eV}$ and $\text{DCNN} (0,0) = 1.176 \pm 0.010 \text{ eV}$.

$1.679 \pm 0.006 \text{ eV}$. Figure 5 is an expanded scan over the $\tilde{A} \ ^2A'$ states of HCNN and DCNN. The complex structure in Figure 5 is reproducible, and we believe that these features are real. There is an irregular progression in $^2A'$ HCNN with splittings of $400\text{--}500 \text{ cm}^{-1}$, but in $^2A'$ DCNN we cannot resolve the small splittings ($\approx 80\text{--}170 \text{ cm}^{-1}$). The origins of the $\tilde{A} \ ^2A'$ states of HCNN and DCNN are not easily assigned, and we can only identify upper bounds for these ions as $1.325 \pm 0.010 \text{ eV} \geq \tilde{A} \ ^2A' \text{ HCNN} (0,0) \geq 1.172 \pm 0.010 \text{ eV}$ and $1.325 \pm 0.010 \text{ eV} \geq \tilde{A} \ ^2A' \text{ DCNN} (0,0) \geq 1.176 \pm 0.010 \text{ eV}$. These origins imply $0.522 \pm 0.012 \text{ eV} \leq T_0(^2A' \text{ HCNN}) \leq 0.675 \pm 0.012 \text{ eV}$ and $0.522 \pm 0.012 \text{ eV} \leq T_0(^2A' \text{ DCNN}) \leq 0.678 \pm 0.012 \text{ eV}$. These complex spectra indicate that there is a large geometry change following detachment of the HCNN^- negative ion to produce the $^2A'$ excited state of HCNN. From the schemes in eq 13, we anticipate that detachment of the HCNN^- anion to produce $\tilde{A} \ ^2A'$ HCNN will strongly excite the H–CNN bending mode, ν_5 . The calculated H–C=NN angle increases from 109.2° in HCNN^- to 147.4° in $\tilde{A} \ ^2A'$ HCNN.



Expression 13 suggests that we might consider $\tilde{A} \ ^2A'$ HCNN to be a wide-amplitude bender (or a “floppy”) radical.³¹

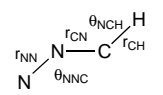
The yields of photodetached electrons are angle dependent. The distribution of scattered photoelectrons $I(\theta)$ is approximated^{32,33} by the following expression.

$$I(\theta) = \frac{\bar{\sigma}}{4\pi} [1 + \beta(E)P_2(\cos\theta)] \quad (14)$$

In this expression, θ is the angle between the polarization of the laser light ($\mathbf{E}_{\text{laser}}$) and the electron collection direction, $\bar{\sigma}$ is the average photodetachment cross section, and $\beta(E)$ is the anisotropy factor which depends on the energy of the scattered electron E . The anisotropy factor $\beta(E)$ can vary from -1 to $+2$ ($-1 \leq \beta \leq 2$). The photoelectron spectra shown in Figures 1–5 are collected under conditions where θ is set to the “magic angle” of 54.7° , where $P_2(\cos\theta) = 0$ so that $I(\theta) = \bar{\sigma}/4\pi$ and is independent of $\beta(E)$. If spectra are collected at $\theta = 0^\circ$ ($\mathbf{E}_{\text{laser}}$ and collection direction \parallel) and $\theta = 90^\circ$ ($\mathbf{E}_{\text{laser}}$ and collection

TABLE 4: Ab Initio Electronic Structure Calculations in a 6-311++G(2df,p) Basis

calculation	energy/au	$\langle S^2 \rangle$	$r_{\text{CN}}/\text{\AA}$	$r_{\text{NN}}/\text{\AA}$	B_e/cm^{-1}	$\mu/D[\delta^-\text{C}=\text{N}=\text{N}^{\delta+}]$
CNN $\tilde{X}^3\Sigma^-$						
ROHF	-146.68125	2.0	1.156	1.289	0.433	0.33
UHF	-146.70539	2.184	1.188	1.228	0.446	1.01
DFT B3LYP	-147.49478	2.035	1.232	1.195	0.441	0.74
CNN $^- \tilde{X}^2\Pi$						
DFT B3LYP	-147.56169	0.764	1.217	1.230	0.435	
Harmonic Vibrational Frequencies (unscaled) and IR Intensities: ω/cm^{-1} [A/km mol $^{-1}$]						
calculation	ω_1/CNN symmetric stretch		ω_2/CNN bend		ω_3/CNN asymmetric stretch	
CNN $\tilde{X}^3\Sigma^-$						
ROHF	CN-N stretch	1079 [41]	329 [0.5]		2270 [364]	
UHF	CN-N stretch	1175 [0.2]	406 [3]		1758 [0.7]	
DFT B3LYP		1283 [16]	409 [7]		1517 [0.3]	
CNN $^- \tilde{X}^2\Pi$						
DFT B3LYP		1211 [134]	522 [9]		1692 [406]	

HCNN						
	HCNN \tilde{X}^2A' (B3LYP/6-311++G(2df,p))		HCNN $^- \tilde{X}^1A'$ (B3LYP/6-311++G(2df,p))			
$r_{\text{NN}}/\text{\AA}$	1.151		1.171			
$r_{\text{NC}}/\text{\AA}$	1.268		1.263			
$r_{\text{CH}}/\text{\AA}$	1.088		1.092			
θ_{NNC}	170.5		172.7			
θ_{NCH}	116.0		114.2			
A_e/cm^{-1}	20.504		19.794			
B_e/cm^{-1}	0.412		0.407			
C_e/cm^{-1}	0.403		0.399			
energy/au	-148.129 54		-148.191 05			
$\langle S^2 \rangle$	0.765		0			
$\mu/D[\delta^-\text{HC}=\text{N}=\text{N}^{\delta+}]$	1.65					
Harmonic Vibrational Frequencies (unscaled) and IR Intensities: ω/cm^{-1} [A/km mol $^{-1}$]						
	$\omega_1(a')$ (C-H stretch)	$\omega_2(a')$ (N-N-CH asymmetric stretch)	$\omega_3(a')$ (N-N-CH symmetric stretch)	$\omega_4(a')$ (NNC-H bend)	$\omega_5(a')$ (N-N-CH bend)	$\omega_6(a'')$ (N-N-CH bend)
HCNN	3147[4]	1879[283]	1258[4]	888[279]	537[26]	486[0.1]
DCNN	2319[6]	1868[320]	1223[29]	740[115]	485[44]	474[3]
HCNN $^-$	3055[57]	1996[1264]	1271[11]	959[186]	558[27]	607[0.4]

direction \perp), one can extract a value for the anisotropy factor.

$$\beta = \frac{I_{0^\circ} - I_{90^\circ}}{1/2 I_{0^\circ} + I_{90^\circ}} \quad (15)$$

The value of β provides an important clue as to the nature of the photodetached electron. For atoms, detachment of an s electron leads to an outgoing p-wave ($l=1$) and $\beta = +2$, independent of the electron kinetic energy. Detachment of a p electron results in a mixture of interfering s- and d- waves and leads to an energy dependent value for $\beta(E)$. At the photodetachment threshold, s-wave ($l=0$) detachment dominates giving $\beta = 0$ and yielding an isotropic photoelectron angular distribution. At photoelectron kinetic energies roughly 1 eV above threshold, d-wave detachment becomes important and $\beta \rightarrow -1$. Electron detachment from molecular ions is more complicated than the atomic case, but β is generally found to be positive for detachment for σ (s-like) electrons and negative for detachment for π (p-like) electrons.

Use of (15) leads to the following anisotropy factors; $\beta(\text{CNN}, ^3\Sigma^-; 1.76 \text{ eV kinetic energy}) = -0.91 \pm 0.15$ and $\beta(\text{CNN}, ^1\Delta; 0.92 \text{ eV kinetic energy}) = -0.43 \pm 0.15$; $\beta(\text{HCNN}, ^2A''; 1.85 \text{ eV kinetic energy}) = -0.84 \pm 0.15$. All of these β values are suggestive of ejection of a π -like electron from both the CNN $^-$

and HCNN $^-$ anions and are in qualitative agreement with our pictures of these negative ions in (7) and (9). Furthermore, we measure $\beta(\text{HCNN}, ^2A'; 1.17 \text{ eV kinetic energy}) = 0.0 \pm 0.15$. This is consistent with detachment of an electron from the σ -like "lobe orbital" of HCNN $^- \tilde{X}^1A'$ in (13), which has a different shape than the high-lying π -like orbital of HCNN $^-$.

In order to aid in the interpretation of the photoelectron spectra, we have carried out a uniform set of ab initio electronic structure calculations on diazocarbene and the diazomethyl radical as well as their corresponding anions. Our calculations are DFT/B3LYP computations³⁴ in a 6-311++G(2df,p) basis and they are reported in Table 4.

B. Negative Ion Chemistry. Studies of the reactions of the diazomethide and diazocarbene ions were made with the FTMS over the course of several days and $k_{11} = (2.02 \pm 0.11) \times 10^{-10} \text{ cm}^3 \text{ s}^{-1}$ while $k_{-11} = (3.96 \pm 0.52) \times 10^{-10} \text{ cm}^3 \text{ s}^{-1}$. The given error represents the standard deviation of nine and eight observations, respectively; the average correlation coefficient (r^2) for all of the kinetic plots was 0.995. It is unlikely, however, that the absolute error for this type of measurement is less than 20%, primarily because of the difficulty in accurately determining the pressure of the neutral compound. Therefore, this larger uncertainty was used to propagate the error and $K_{\text{equi-}}(11) = 0.51 \pm 0.14$ while $\Delta_{\text{rxn}}G_{298}(11) = 0.40 \pm 0.12 \text{ kcal mol}^{-1}$.

TABLE 5: Acidity Data for the Proton Affinity of CNN^- : $\text{HA} + \text{CNN}^- \rightarrow \text{A}^- + \text{HCNN}^a$

HA	$\Delta_{298}H_{\text{acid}}(\text{HA})$	proton transfer		FA-SIFT rates	
		FTMS	FA-SIFT	$k_{\text{TOTAL}}/\text{cm}^3 \text{ s}^{-1}$	yield $[\text{A}^-]/\text{loss}[\text{CNN}^-]$
<i>m</i> -methylaniline	366.8 ± 2.1	—	—	—	—
$\text{CF}_3\text{CH}_2\text{OH}$	361.9 ± 2.5	—	—	—	—
pyrrole	358.7 ± 2.2	—	—	—	—
CH_3SH	356.9 ± 2.2	—	—	1.1×10^{-9}	0%
$\text{CH}_3\text{CH}_2\text{SH}$	355.2 ± 2.2	—	—	1.5×10^{-9}	0%
4-methylpyrazole	354.8 ± 2.1	—	—	—	—
pyrazole	353.8 ± 2.1	—	—	—	—
$(\text{CH}_3)_3\text{CSH}$	352.5 ± 2.2	+	+	1.4×10^{-9}	~2–3% ^b
$\text{CH}_3\text{CO}_2\text{H}$	348.6 ± 2.9	+	+	1.0×10^{-9}	~25% ^b

^a All acidity values are in kcal mol⁻¹ and were taken from Lias et al.³⁸ The observation or nonobservance of A^- indicated by +, —. ^b Corrections for mass discrimination would increase these values slightly.

In order to obtain the proton affinity of CHN_2^- , or equivalently $\Delta_{\text{acid}}H_{298}(\text{CH}_2\text{N}_2)$, the change in entropy, $\Delta_{\text{rxn}}S_{298}(11)$ is needed. This was determined to be $\Delta_{\text{rxn}}S_{298}(11) = 1.17 \text{ cal mol}^{-1} \text{ K}^{-1}$ and was obtained as the sum of the translational, rotational, and vibrational contributions for each species using standard statistical mechanics expressions.^{35,36} Rotational constants and frequencies used in these formulas were taken from HF/6-31+G(d) calculations and the latter values were scaled³⁷ by an empirical factor of 0.893. The resulting $\Delta_{\text{rxn}}H_{298}(0.75 \pm 0.12 \text{ kcal mol}^{-1})$ was combined³⁸ with $\Delta_{\text{acid}}H_{298}(\text{CH}_3\text{CN}) = 372.9 \pm 2.1$ to yield the enthalpy of deprotonation of diazomethane: $(\Delta_{\text{acid}}H_{298}(\text{CH}_2\text{N}_2) = 372.2 \pm 2.1 \text{ kcal mol}^{-1})$.

Bracketing experiments with the CNN^- ion have been carried out with a variety of acids in the FTMS to determine the proton affinity, PA, of the ion. For both thiomethanol and thioethanol, the conjugate base RS^- is detected but it is present even when the *m/z* 40 ion (CNN^-) is ejected from the cell and when diazomethane is omitted from the experiment. A fast reaction between the thiol and CNN^- does take place leading to a significant amount of signal loss. The thiolate intensity does not increase with time, however; therefore, proton transfer does not appear to be taking place. For proton transfer with $(\text{CH}_3)_3\text{CSH}$, the $(\text{CH}_3)_3\text{CS}^-$ signal only slowly grows in with time. Proton transfer with acetic acid is observed to occur. These results are summarized in Table 5 and indicate that $\text{PA}(\text{CNN}^-) \equiv \Delta_{298}H_{\text{acid}}(\text{HCN}_2)$ is $352 \text{ kcal mol}^{-1}$.

In the FA-SIFT instrument the CNN^- anion undergoes rapid reaction with CH_3SH , $\text{C}_2\text{H}_5\text{SH}$, $(\text{CH}_3)_3\text{CSH}$ and $\text{CH}_3\text{CO}_2\text{H}$; the reaction rate constants and product distributions are summarized in Table 5. For both CH_3SH and $\text{C}_2\text{H}_5\text{SH}$, no product ions are observed and exothermic reactive detachment processes are presumed to occur (e.g., $\text{CNN}^- + \text{CH}_3\text{SH} \rightarrow \text{H}_2\text{CNN} + \text{CH}_2\text{S} + \text{e}^-$). For both $(\text{CH}_3)_3\text{CSH}$ and $\text{CH}_3\text{CO}_2\text{H}$, the conjugate bases [$(\text{CH}_3)_3\text{CS}^-$ and CH_3CO_2^- respectively], are formed by proton transfer. For reactions of acetic acid, clusters [$\text{CH}_3\text{CO}_2^-(\text{CH}_3\text{CO}_2\text{H})$] were also observed; no other ions were detected. The FTMS and FA-SIFT results indicate that $\Delta_{298}H_{\text{acid}}(\text{HCN}_2) = 352 \pm 4 \text{ kcal mol}^{-1}$, where the conservative error bars reflect uncertainties in the acidity values of the bracketing compounds as well as the occurrence of processes in competition with proton transfer. These experimental data provide no information as to which end of CNN^- is protonated (i.e., C vs. N).

IV. Thermochemistry

In order to gain insight into the chemistry of C and CH with N_2 , we need to establish the thermochemistry of CNN and HCNN. Our negative ion results enable us to determine most of the thermodynamics of these reactive intermediates.

The chemistry and spectroscopy of negative ions provides a useful avenue to extract a number of thermochemical parameters.³⁹ If one can measure the enthalpy of deprotonation for a species RH, [$\Delta_{\text{acid}}H_{298}(\text{RH})$], and separately find the electron affinity of the corresponding radical, [$\text{EA}(\text{R})$], then a simple cycle that uses the ionization potential of H atom can provide a value for the bond enthalpy [$DH_{298}(\text{RH})$].

$$\Delta_{\text{acid}}H_{298}(\text{RH}) = DH_{298}(\text{RH}) + \text{IP}(\text{H}) - \text{EA}(\text{R}) - \int_0^{298} dT[C_p(\text{R}) - C_p(\text{R}^-) + C_p(\text{H}) - C_p(\text{H}^+)] \quad (16)$$

Since the sum of the integrated heat capacities is always small ($\leq 0.3 \text{ kcal mol}^{-1}$),³⁹ the term in brackets can be ignored and we will use a more common expression, $\Delta_{\text{acid}}H_{298}(\text{RH}) \cong DH_{298}(\text{RH}) + \text{IP}(\text{H}) - \text{EA}(\text{R})$.

The gas-phase acidity of diazomethane was measured previously in a flowing afterglow device⁴⁰ and the enthalpy of deprotonation ($373 \pm 3 \text{ kcal/mol}$) is in excellent accord with our determination of $\Delta_{\text{acid}}H_{298}(\text{H}-\text{CHNN}) = 372.2 \pm 2.1 \text{ kcal/mol}$. Use of the electron affinity, $\text{EA}(\text{HCNN}) = 38.9 \pm 0.1 \text{ kcal mol}^{-1}$, leads to a value for the bond enthalpy of diazomethane, $DH_{298}(\text{H}-\text{CHNN}) = 97 \pm 2 \text{ kcal mol}^{-1}$. The bond enthalpy at 298 K and the bond energy at 0 K are related by the heat capacities.

$$DH_{298}(\text{RH}) = D_0(\text{RH}) + \int_0^{298} dT[C_p(\text{R}) + C_p(\text{H}) - C_p(\text{RH})] \cong D_0(\text{RH}) + \int_0^{298} dT C_p(\text{H}) \quad (17)$$

Since the integrated heat capacity for H atom is $5/2 RT$, we estimate $D_0(\text{H}-\text{CHNN}) = 96 \pm 2 \text{ kcal mol}^{-1}$.

There have been several experimental determinations of the $\Delta_f H_0(\text{CH}_2\text{N}_2)$. Photochemical studies⁴¹ of CH_2N_2 imply $\Delta_f H_0(\text{CH}_2\text{N}_2) \geq 51.3 \text{ kcal mol}^{-1}$ and Benson⁴² tabulates a value, $\Delta_f H_{300}(\text{CH}_2\text{N}_2) = 71 \text{ kcal mol}^{-1}$. Recent ab initio electronic structure calculations (G2) have established the energetics of diazomethane.⁴³ The G2 calculations and CBS ab initio results (vide infra) are in agreement, and we adopt the CBS-QCI/APNO values: $\Delta_f H_0(\text{CH}_2\text{N}_2) = 65.7 \pm 0.7 \text{ kcal mol}^{-1}$ and $\Delta_f H_{298}(\text{CH}_2\text{N}_2) = 64.1 \pm 0.7 \text{ kcal mol}^{-1}$. Consequently our experimental values for $DH_{298}(\text{H}-\text{CHNN})$ and $D_0(\text{H}-\text{CHNN})$ lead to the heats of formation: $\Delta_f H_0(\text{HCNN}) = 110.4 \pm 2.0 \text{ kcal mol}^{-1}$ and $\Delta_f H_{298}(\text{HCNN}) = 109.8 \pm 2.0 \text{ kcal mol}^{-1}$.

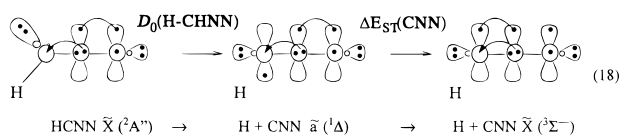
The energetics of diazocarbene could be established if we had a reliable value for $\Delta_{\text{acid}}H_{298}(\text{HCNN})$. The FTMS and FA-SIFT results (vide supra) both indicate that $\Delta_{\text{acid}}H_{298}(\text{HCNN})$

TABLE 6: Energetics of Diazomethyl Radical and Diazocarbene

HCNN			
EA(\tilde{X}^2A'' HCNN)/eV	1.685 ± 0.006	(38.9 ± 0.1 kcal mol ⁻¹)	
$\Delta_{\text{acid}}H_{298}(\text{CH}_2\text{N}_2)$ /kcal mol ⁻¹	372 ± 2		
$DH_{298}(\text{H}-\text{CHNN})$ /kcal mol ⁻¹	97 ± 2		
$D_0(\text{H}-\text{CHNN})$ /kcal mol ⁻¹	96 ± 2		
$\Delta_f H_0(\text{H}_2\text{CNN})$ /kcal mol ⁻¹	66 ± 1	$\Delta_f H_{298}(\text{H}_2\text{CNN})$ /kcal mol ⁻¹	64 ± 1
$\Delta_f H_0(\text{HCNN})$ /kcal mol ⁻¹	110 ± 2	$\Delta_f H_{298}(\text{HCNN})$ /kcal mol ⁻¹	110 ± 2
$T_0(\tilde{A}^2A' \text{ HCNN})$ /eV	0.522 ± 0.012 ≤ T_0 ≤ 0.675 ± 0.012		
$T_0(\text{HCNN})$ /eV	3.78		ref 15
CNN			
EA($\tilde{X}^3\Sigma^-$ CNN)/eV	1.771 ± 0.010	(40.8 ± 0.2 kcal mol ⁻¹)	
$\Delta_{\text{acid}}H_{298}(\text{HCNN})$ /kcal mol ⁻¹	352 ± 4		
$DH_{298}(\text{H}-\text{CNN})$ /kcal mol ⁻¹	79 ± 4		
$D_0(\text{H}-\text{CNN})$ /kcal mol ⁻¹	78 ± 4		
$\Delta_f H_0(\text{CNN})$ /kcal mol ⁻¹	136 ± 5	$\Delta_f H_{298}(\text{CNN})$ /kcal mol ⁻¹	136 ± 5
$T_0(\tilde{a}^1\Delta \text{ CNN})$ /eV	0.846 ± 0.014		
$T_0(\tilde{b}^1\Sigma^+ \text{ CNN})$ /eV	1.325 ± 0.015		
$T_0(\tilde{A}^3\Pi \text{ CNN})$ /eV	2.957 ± 0.001		ref 14
$T_0(\tilde{B}^3\Sigma^-/\text{Ar matrix CNN})$ /eV	≤ 4.95		ref 15
$T_0(\tilde{C}^3\Pi/\text{Ar matrix CNN})$ /eV	6.02		ref 15

is 352 ± 4 kcal mol⁻¹. The experimental EA(CNN) of 40.8 ± 0.2 kcal mol⁻¹ gives $DH_{298}(\text{H}-\text{CNN}) = 79 \pm 4$ kcal mol⁻¹ and $D_0(\text{H}-\text{CNN}) = 78 \pm 4$ kcal mol⁻¹. The corresponding heats of formation are: $\Delta_f H_0(\text{CNN}) = 136 \pm 5$ kcal mol⁻¹ and $\Delta_f H_{298}(\text{CNN}) = 136 \pm 5$ kcal mol⁻¹. These heats of formation for diazocarbene are within the (large) uncertainties reported⁴⁴ earlier: $\Delta_f H_0(\text{CNN}) = 151 \pm 24$ kcal mol⁻¹ and $\Delta_f H_{298}(\text{CNN}) = 151 \pm 24$ kcal mol⁻¹.

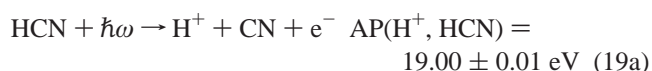
The experimental thermochemistry reveals that the successive C–H bonds in diazomethane differ in strength: $D_0(\text{H}-\text{CHNN}) = 96 \pm 2$ kcal mol⁻¹ and $D_0(\text{H}-\text{CNN}) = 78 \pm 4$ kcal mol⁻¹. This is reminiscent of our earlier finding⁴⁵ for cyanamide: $DH_{298}(\text{H}-\text{NHCHN}) = 97 \pm 3$ kcal mol⁻¹ and $DH_{298}(\text{H}-\text{NCN}) = 83 \pm 2$ kcal mol⁻¹. In the absence of interactions between the two unpaired electrons in CNN, the first and second C–H bond energies in diazomethane would be expected to be comparable.^{46,47} The fact that the second C–H bond is much weaker than the first indicates that there is significant coupling between the unpaired electrons, as one would expect given nitrene/carbene structures shown in expression 5. The C–H bond energy of the diazomethyl radical can be related that of diazomethane: $D_0(\text{H}-\text{CNN}) = D_0(\text{H}-\text{CHNN}) - \Delta E_{\text{ST}}(\text{CNN})$. Using the thermochemical results described above and the singlet/triplet energy from the photoelectron spectrum [$\Delta E(^1\Delta - ^3\Sigma^-) = 0.846$ eV], we estimate $D_0(\text{H}-\text{CNN}) \cong 77 \pm 2$ kcal mol⁻¹.



In order to consider the energetics of reaction 3, accurate thermochemistry of CH and HCN is essential. Optical studies of the excited electronic states of CH have been reported which examined the fluorescence: $\text{CH}^* \rightarrow \text{CH X } ^2\Pi$. Predissociation⁴⁸ shortens the life of the $B^2\Sigma^-$ and $C^2\Sigma^+$ states of CH emitting to $\text{CH(X } ^2\Pi)$. Analysis of the line broadening leads to $D_0(\text{CH X } ^2\Pi) = 27\,950 \pm 80$ cm⁻¹, which is a small improvement over the earlier value⁴⁹ of Herzberg and Johns of $D_0(\text{CH X } ^2\Pi) = 27\,856 \pm 100$ cm⁻¹. Ion spectroscopy has provided an independent check of this dissociation energy. Photofragment spectroscopy⁵⁰ of $\text{CH}^+(\text{A}^1\Pi) \leftarrow \text{CH}^+(\text{X}^1\Sigma^+)$, followed by dissociation $\text{CH}^+(\text{A}^1\Pi) \rightarrow \text{C}^+(\text{ } ^2P) + \text{H}(\text{ } ^2S)$, yielded the dissociation energies of CH^+ : $D_0(\text{CH}^+ \text{ X } ^1\Sigma^+) =$

$32\,907 \pm 23$ cm⁻¹ and $D_0(\text{CH}^+ \text{ A}^1\Pi) = 9\,351 \pm 23$ cm⁻¹. There is a thermochemical cycle which relates the properties of CH and CH^+ : $D_0(\text{CH}^+ \text{ X } ^1\Sigma^+) + \text{IP}(\text{CH}) = D_0(\text{CH X } ^2\Pi) + \text{IP}(\text{C})$. Use⁵¹ of the $\text{IP}(\text{C})$ and⁵⁰ $\text{IP}(\text{CH}) = 85\,850 \pm 100$ cm⁻¹ yields the dissociation energy: $D_0(\text{CH X } ^2\Pi) = 27\,937 \pm 120$ cm⁻¹. Here we adopt $D_0(\text{CH X } ^2\Pi) = 27\,950 \pm 80$ cm⁻¹ and use $\Delta_f H_0(\text{CH X } ^2\Pi) = 141.7 \pm 0.1$ kcal mol⁻¹ and $\Delta_f H_{298}(\text{CH X } ^2\Pi) = 142.5 \pm 0.2$ kcal mol⁻¹.

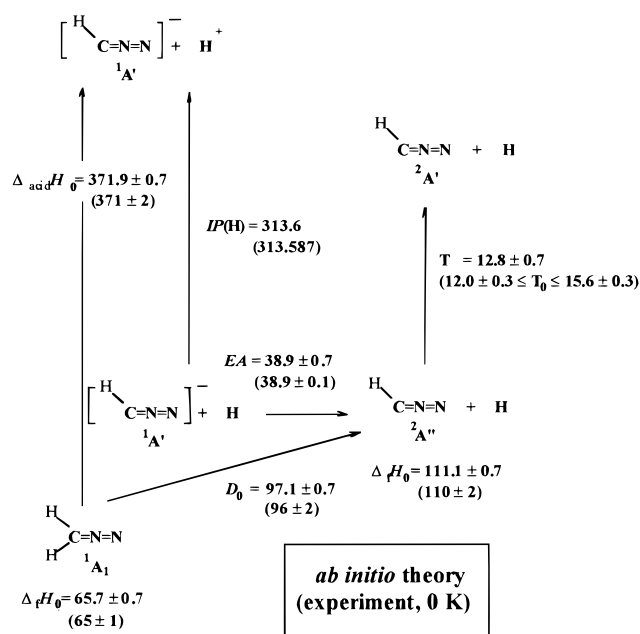
Finally we require accurate thermochemistry of HCN to complete the energetics of reaction 3. The heat of formation of HCN is given by standard tables⁴⁴ as $\Delta_f H_0(\text{HCN}) = 132.384 \pm 4$ kJ mol⁻¹ or 31.6 ± 1.0 kcal mol⁻¹. We can improve this value by using recent values of the photoionization appearance potential,⁵² the photodissociation threshold,⁵³ and the photoion-pair appearance potential⁵⁴/electron affinity⁵⁵ of CN together with a new $\Delta_f H_0(\text{CN})$ derived from the photodissociation of cyanogen:⁵⁶



Measurements of reactions 19a, 19b, and 19c yield HCN dissociation energies of $D_0(\text{H}-\text{CN}) = 124.6 \pm 0.2$, 125.1 ± 0.4 , and 125.5 ± 0.5 kcal mol⁻¹, respectively. The more precise values are those of reactions 19a and 19b. We adopt an average value of $D_0(\text{H}-\text{CN}) = 124.8 \pm 0.5$ kcal mol⁻¹ and use a recent⁵⁶ heat of formation of CN of $\Delta_f H_0(\text{CN}) = 104.1 \pm 0.5$ kcal mol⁻¹ and recommend $\Delta_f H_0(\text{HCN}) = 30.9 \pm 0.7$ kcal mol⁻¹ and $\Delta_f H_{298}(\text{HCN}) = 30.8 \pm 0.7$ kcal mol⁻¹ (as well as $DH_{298}(\text{H}-\text{CN}) = 126.3 \pm 0.9$ kcal mol⁻¹). These heats of formation are a small improvement over the currently accepted values⁴⁴ of $\Delta_f H_0(\text{HCN}) = 31.6 \pm 1.0$ kcal mol⁻¹ and $\Delta_f H_{298}(\text{HCN}) = 31.5 \pm 1.0$ kcal mol⁻¹. Much of the thermochemistry of the diazomethyl radical and diazocarbene is summarized in Tables 6 and 7.

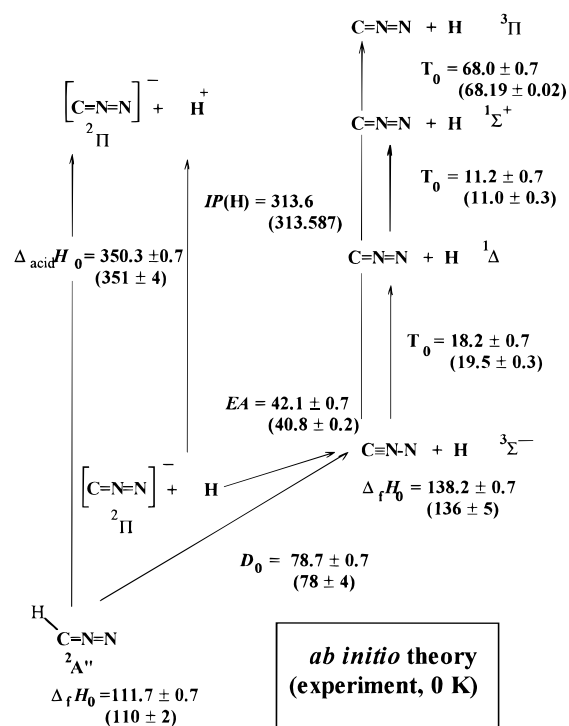
TABLE 7: Experimental Thermochemistry of Diazomethyl Radical and Diazocarbene

process		$\Delta_{\text{rxn}}H_0/\text{kcal mol}^{-1}$	$\Delta_{\text{rxn}}H_{298}/\text{kcal mol}^{-1}$	ref
$\text{N}_2(^1\Sigma_g^+)$	$\rightarrow \text{N}(^4S_{3/2}) + \text{N}(^4S_{3/2})$	225.06 ± 0.03	225.95 ± 0.03	71
$\text{HCN}(^1\Sigma^+)$	$\rightarrow \text{H} + \text{CN}(^2\Sigma^+)$	125.1 ± 0.7	126.3 ± 0.9	this work
$\text{HCN}(^1\Sigma^+)$	$\rightarrow \text{HC}(^2\Pi) + \text{N}(^4S)$	223.2 ± 0.7	224.7 ± 0.7	this work
$\text{HCN}(^1\Sigma^+)$	$\rightarrow \text{HC}(^4\Sigma^-) + \text{N}(^4S)$	240.5 ± 0.7	241.8 ± 0.7	this work
$\text{CN}(^2\Sigma^+)$	$\rightarrow \text{C}(^3P) + \text{N}(^4S)$	178.4 ± 0.6	179.3 ± 0.6	56,71
$\text{HC}(^2\Pi) + \text{N}_2(^1\Sigma_g^+)$	$\rightarrow \text{HCN}(^1\Sigma^+) + \text{N}(^4S)$	1.6 ± 0.7	1.3 ± 0.9	this work
$\text{HC}(^4\Sigma^-) + \text{N}_2(^1\Sigma_g^+)$	$\rightarrow \text{HCN}(^1\Sigma^+) + \text{N}(^4S)$	-15.2 ± 0.9	-15.6 ± 0.9	this work
$\text{HCCH}(^1\Sigma_g^+)$	$\rightarrow \text{HCC}(^2\Sigma^+) + \text{H}$	131.3 ± 0.7	132.8 ± 0.7	72
$\text{HCCH}(^1\Sigma_g^+)$	$\rightarrow \text{HC}(^2\Pi) + \text{CH}(^2\Pi)$	228.9 ± 0.8	230.7 ± 0.3	44
$\text{CO}(^1\Sigma^+)$	$\rightarrow \text{C}(^3P_0) + \text{O}(^3P_2)$	256.2 ± 0.1	257.3 ± 0.1	71
$\text{H}_2\text{CNN}(^1A_1)$	$\rightarrow \text{H} + \text{HCNN}(^2A'')$	97 ± 3	98 ± 3	this work
$\text{H}_2\text{CNN}(^1A_1)$	$\rightarrow \text{CH}_2(^3B_1) + \text{N}_2(^1\Sigma_g^+)$	27 ± 1	29 ± 1	this work
$\text{HCNN}(^2A'')$	$\rightarrow \text{HC}(^2\Pi) + \text{N}_2(^1\Sigma_g^+)$	31 ± 3	33 ± 3	this work
$\text{HCNN}(^2A'')$	$\rightarrow \text{HC}(^4\Sigma^-) + \text{N}_2(^1\Sigma_g^+)$	48 ± 3	50 ± 3	this work
$\text{HCNN}(^2A'')$	$\rightarrow \text{HCN}(^1\Sigma^+) + \text{N}(^4S)$	34 ± 3	35 ± 3	this work
$\text{HCNN}(^2A'')$	$\rightarrow \text{CNN}(^3\Sigma^-) + \text{H}$	78 ± 4	79 ± 4	this work
$\text{HCNN}(^2A'')$	$\rightarrow \text{HCN}(^2A'')$	-31 ± 3	-33 ± 4	this work, 45
$\text{CNN}(^3\Sigma^-)$	$\rightarrow \text{CN}(^2\Sigma^+) + \text{N}(^4S)$	83 ± 4	84 ± 3	this work
$\text{CNN}(^3\Sigma^-)$	$\rightarrow \text{C}(^3P) + \text{N}_2(^1\Sigma_g^+)$	37 ± 3	36 ± 3	this work
$\text{CNN}(^3\Sigma^-)$	$\rightarrow \text{NCN}(^3\Sigma_g^-)$	-24 ± 4	-26 ± 4	this work, 45

CBS-APNO Calculations and Experiment/kcal mol⁻¹Figure 6. Calculated CBS-QCI/APNO ab initio thermochemical cycle for H_2CNN . The experimental results are given in parentheses for comparison.

V. Complete Basis Set ab Initio Electronic Structure Calculations

All of the generalized valence bond formulas in equations 5–9 are qualitatively correct; the shapes of the radicals and ions as well as the order of the electronic states are correctly predicted. The rotational constants and harmonic vibrational frequencies are also faithfully rendered by the DFT-B3LYP calculations. The small number of atoms in the two systems allowed us to perform the full range of computationally intensive complete basis set (CBS) calculations.^{34,57,58} These compound models employ modest basis sets for the geometry and frequency calculations, large basis sets for a single-point SCF calculation, medium basis sets for the MP2 correction with extrapolation to the CBS limit, and small basis sets for higher orders of perturbation theory. The most demanding CBS-QCI/APNO model employs atomic pair natural orbital (APNO) basis sets, while the CBS-Q model goes up to QCISD(T)/6-31+G⁺⁺

CBS-APNO Calculations and Experiment/kcal mol⁻¹Figure 7. Calculated CBS-QCI/APNO ab initio thermochemical cycle for HCNN . The experimental results are given in parentheses for comparison.

calculations, and the CBS-4 model tops off at MP4/6-31G. These CBS-QCI/APNO, CBS-Q, and CBS-4 models are applicable to systems with up to 4, 8, and 16 many-electron atoms with root mean square (rms) errors of ± 0.7 , ± 1.3 , and ± 2.5 kcal mol⁻¹ respectively.^{34,57,58} The results are summarized in Table 8 where the uncertainties quoted are the rms errors from the G2 test set.⁵⁹ The agreement between our experimental findings and the results of these ab initio electronic structure calculations is excellent, but the performance of the relatively inexpensive CBS-4 model is disappointing (Table 9).

The HCNN^- CBS-QCI/APNO results are shown in Figure 6 while those for CNN^- are displayed in Figure 7. For diazocarbene, a CASSCF(2,4)-MP2/6-311G(2df,p) calculation was used to compute $\Delta E(^1\Delta, ^1\Sigma^+)$ for CNN . All calculations

TABLE 8: Complete Basis Set (CBS) Calculated ab Initio Electronic Energies

molecule	state	method	energy/hartree	$\Sigma D_0/\text{kcal mol}^{-1}$	$\Delta_f H_0/\text{kcal mol}^{-1}$	$\Delta_f H_{298}/\text{kcal mol}^{-1}$
C	3P	CBS-4	-37.788 25			
		CBS-Q	-37.785 15			
		CBS-QCI/APNO	-37.842 08			
CH	$^2\Pi$	CBS-4	-38.418 41	79.6 ± 2.5	142.0 ± 2.5	142.9 ± 2.5
		CBS-Q	-38.412 14	79.8 ± 1.3	141.8 ± 1.3	142.6 ± 1.3
		CBS-QCI/APNO	-38.469 30	79.8 ± 0.7	141.8 ± 0.7	142.6 ± 0.7
N ₂	$^1\Sigma_g^+$	CBS-4	-109.400 01	220.3 ± 2.5		
		CBS-Q	-109.396 03	223.1 ± 1.3		
		CBS-QCI/APNO	-109.527 48	223.8 ± 0.7		
CNN	$^3\Pi$	CBS-4	-147.142 84	191.8 ± 2.5	203.3 ± 2.5	203.5 ± 2.5
		CBS-Q	-147.129 08	190.4 ± 1.3	204.6 ± 1.3	205.0 ± 1.3
		CBS-QCI/APNO	-147.313 74	188.8 ± 0.7	206.2 ± 0.7	206.6 ± 0.7
	$^1\Sigma^+$	CBS-4	-147.191 23	222.1 ± 2.5	172.9 ± 2.5	173.0 ± 2.5
		CBS-Q	-147.190 18	228.7 ± 1.3	166.3 ± 1.3	166.4 ± 1.3
		CBS-QCI/APNO	-147.375 33	227.5 ± 0.7	167.6 ± 0.7	167.7 ± 0.7
	$^1\Delta$	CBS-4	-147.209 02	233.27 ± 2.5	161.8 ± 2.5	161.9 ± 2.5
		CBS-Q	-147.207 97	239.90 ± 1.3	155.1 ± 1.3	155.2 ± 1.3
		CBS-QCI/APNO	-147.393 11	238.62 ± 0.7	156.4 ± 0.7	156.5 ± 0.7
	$^3\Sigma^-$	CBS-4	-147.242 05	254.0 ± 2.5	141.0 ± 2.5	141.2 ± 2.5
		CBS-Q	-147.236 37	257.7 ± 1.3	137.3 ± 1.3	137.5 ± 1.3
		CBS-QCI/APNO	-147.422 15	256.8 ± 0.7	138.2 ± 0.7	138.4 ± 0.7
NCN	$^3\Sigma_g^-$	CBS-4	-147.296 43	288.1 ± 2.5	106.9 ± 2.5	107.0 ± 2.5
		CBS-Q	-147.286 47	289.2 ± 1.3	105.9 ± 1.3	106.1 ± 1.3
		CBS-QCI/APNO	-147.470 19	287.0 ± 0.7	108.1 ± 0.7	108.2 ± 0.7
CNN ⁻	$^2\Pi$	CBS-4	-147.304 28			
		CBS-Q	-147.303 16			
		CBS-QCI/APNO	-147.489 28			
H-C< N N	$^2A'$	CBS-4	-147.839 53	313.1 ± 2.5	133.6 ± 2.5	132.7 ± 2.5
		CBS-Q	-147.820 47	310.6 ± 1.3	136.1 ± 1.3	135.1 ± 1.3
		CBS-QCI/APNO	-148.008 88	311.3 ± 0.7	135.4 ± 0.7	134.4 ± 0.7
HCNN	$^2A'$	CBS-4	-147.855 61	323.2 ± 2.5	123.5 ± 2.5	122.9 ± 2.5
		CBS-Q	-147.839 29	322.4 ± 1.3	124.3 ± 1.3	123.6 ± 1.3
		CBS-QCI/APNO	-148.027 17	322.8 ± 0.7	123.9 ± 0.7	123.3 ± 0.7
H-C< N N	2A_2	CBS-4	-147.866 07	329.7 ± 2.5	116.9 ± 2.5	116.1 ± 2.5
		CBS-Q	-147.851 42	330.0 ± 1.3	116.6 ± 1.3	115.8 ± 1.3
		CBS-QCI/APNO	-148.036 87	328.9 ± 0.7	117.8 ± 0.7	116.9 ± 0.7
HCNN	$^2A''$	CBS-4	-147.875 36	335.6 ± 2.5	111.1 ± 2.5	110.6 ± 2.5
		CBS-Q	-147.858 48	334.5 ± 1.3	112.2 ± 1.3	111.6 ± 1.3
		CBS-QCI/APNO	-148.047 49	335.5 ± 0.7	111.1 ± 0.7	110.5 ± 0.7
HCNN ⁻	$^1A'$	CBS-4	-147.945 05			
		CBS-Q	-147.923 05			
		CBS-QCI/APNO	-148.109 45			
H ₂ CNN	1A_1	CBS-4	-148.533 76	432.9 ± 2.5	65.5 ± 2.5	63.8 ± 2.5
		CBS-Q	-148.515 25	433.0 ± 1.3	65.4 ± 1.3	63.8 ± 1.3
		CBS-QCI/APNO	-148.702 15	432.6 ± 0.7	65.7 ± 0.7	64.1 ± 0.7

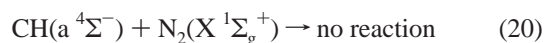
TABLE 9: Comparison of CBS and Experimental Thermochemistry

	CBS ab initio calculated property/kcal mol ⁻¹			experimental/kcal mol ⁻¹
	CBS-4	CBS-Q	CBS-QCI/APNO	
$D_0(\text{H}-\text{CHNN})$	97.3 ± 2.5	98.5 ± 1.3	97.1 ± 0.7	96 ± 2
$\Delta_{\text{acid}}H_{298}(\text{HCHNN})$	370.9 ± 2.5	373.1 ± 1.3	373.4 ± 0.7	372.2 ± 2.1
$\text{EA}(\text{HCNN})$	43.7 ± 2.5	40.5 ± 1.3	38.9 ± 0.7	38.9 ± 0.1
$D_0(\text{HCNN})$	81.6 ± 2.5	76.8 ± 1.3	78.7 ± 0.7	78 ± 4
$\Delta_{\text{acid}}H_{298}(\text{HCNN})$	359.8 ± 2.5	349.9 ± 1.3	351.8 ± 0.7	352 ± 4
$\text{EA}(\text{CNN})$	39.1 ± 2.5	41.9 ± 1.3	42.1 ± 0.7	40.8 ± 0.2

employed a modified version of the Gaussian 94 suite of ab initio electronic structure programs.³⁴

VI. Mechanistic Implications for the Cleavage of N₂ by CH

With the establishment of much of the thermochemistry of diazomethyl radical, it is tempting to speculate on the mechanisms for the “splitting” of N₂. The spin-forbidden reaction 3 has been the subject of numerous investigations. Several groups² have studied the kinetics of CH reaction with N₂ and it is known that only the ground state, CH(X $^2\Pi$), reacts.⁶⁰



A summary³ of these experimental data suggests the formation of an HCNN adduct at temperatures below 1000 K characterized

by a “negative activation energy” of $-2.3 \text{ kcal mol}^{-1}$. The mechanism changes at higher temperatures and shock tube studies suggest the presence of a high-energy HCN + N channel. This high-temperature ($T \geq 2500 \text{ K}$) channel is fit by a normal Arrhenius expression, $k_{\text{obs}} = 7.31 \times 10^{12} \exp(-21970/RT)$ so the activation energy is roughly 22 kcal mol^{-1} .

All recent ab initio electronic structure calculations^{61–64} find two different [CH,N₂] complexes; a dative, linear species, [HCNN], or the diazirnyl radical, *cyclo*-HCN₂,



Extensive molecular dynamics calculations of the insertion path for this spin-forbidden reaction have been reported.^{65,66}

Several early mechanistic schemes^{2,16,67} simply combined CH + N₂ to form a “dative complex”, $^2[\text{HC}-\text{NN}]$, which directly

[NN + CH] Dative Complex
vs. Insertion Complex

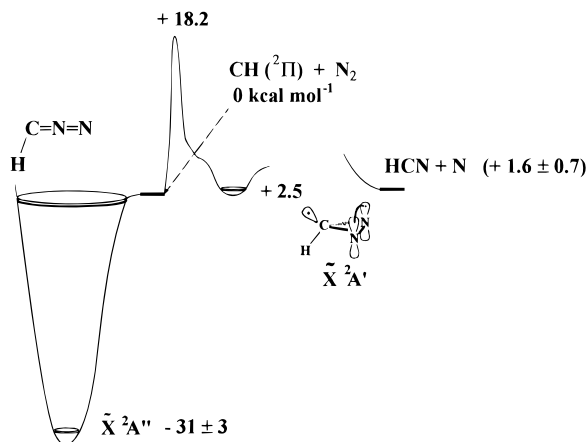
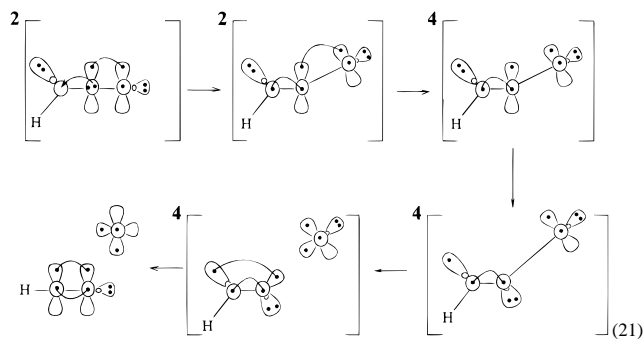


Figure 8. The energetics of the [CH,N₂] dative adduct are contrasted with the [CH,N₂] insertion complex; all values in kcal mol⁻¹. Because $\tilde{X} (^2A'')$ HCNN is bound by 31 kcal mol⁻¹ with respect to [CH + N₂] and the barrier to CH insertion is estimated to be 18 kcal mol⁻¹, a $\tilde{X} (^2A'')$ / $\tilde{a} (^4A'')$ HCNN curve crossing below 50 kcal mol⁻¹ will lead to formation of HCN + N from the $\tilde{X} (^2A'')$ HCNN complex.

crossed over to the quartet surface, ⁴[HCNN], and dissociated to HCN and N atom. The current thermochemistry of HCNN supports this simple mechanism. As CH(²Π) collides with N₂ it is possible for $\tilde{X} (^2A'')$ HCNN [$\Delta_{\text{rxn}}H_0 = -31 \pm 3$ kcal mol⁻¹] to be formed. Figure 8 is a sketch of the CH + N₂ → HCN + N surface which includes the $\tilde{X} (^2A'')$ state of HCNN. All recent ab initio electronic structure calculations⁶³ confirm Bair's conjecture that there is no barrier for the addition: CH + N₂ → HCNN (²A''). We identify Walch's nonplanar *c*-HCN₂ minimum as $\tilde{X} ^2A'$ and have fixed the HCN + N asymptote at the experimental energy of +1.6 ± 0.7 kcal mol⁻¹ (Table 7). Because of the deep well binding HCNN $\tilde{X} (^2A'')$ we believe that the important doublet/quartet crossing to produce HCN + N might not come from the insertion complex, *c*-HCN₂, at all. Instead it may be accessed directly from the dative HCNN species. Table 7 indicates that $\tilde{X} (^2A'')$ HCNN is stable by 31 ± 3 kcal mol⁻¹ with respect to CH + N₂ and is bound by 78 ± 4 kcal mol⁻¹ with respect to H + CNN. The extensive ab initio electronic structure calculations⁶³ estimate that the barrier to CH insertion into N₂ to form the diazirinyl radical is about 18 kcal mol⁻¹ (see Figure 8). We cannot estimate the matrix elements which couple the HCNN doublet states to the quartet manifold, but if the $\tilde{X} (^2A'')$ HCNN surface crossing to a ⁴A'' state is 50 kcal mol⁻¹ or less, then CH insertion into N₂ to produce the diazirinyl radical will not compete. Consequently it might be energetically feasible for N atom elimination to take place directly from $\tilde{X} (^2A'')$ HCNN as shown below in (21).



Acknowledgment. G.B.E. is supported by a grant from the Chemical Physics Program, U.S. Department of Energy (Grant DE-FG02-87ER13695). The collaboration between G.B.E. and G.A.P. is supported via PRF Grant 30676-AC6. Acknowledgment is made to the Donors of the Petroleum Research Fund administered by the American Chemical Society, for partial support of this research. G.A.P. receives support through a grant from Gaussian, Inc. The National Science Foundation is gratefully acknowledged for support to WCL (Grant CHE97-03486 and PHY95-12150). C.H.D., V.M.B., and S.R.K. gratefully acknowledge support of their experimental work by the National Science Foundation (Grants CHE-9421756, CHE-9734867, and CHE-9523415). To carry out the Gaussian 94 ab initio electronic structure calculations, we have used a cluster of RSC-6000 digital computers supported by NSF Grant CHE-9412767. We would particularly like to thank Drs. Trevor Sears and John M. Brown for many fruitful discussions about the spin-orbit and Renner-Teller effects. Drs. Joseph Berkowitz, Thom H. Dunning, Jr., and Larry B. Harding have been very helpful in discussions of the thermochemistry and reaction dynamics of CH.

References and Notes

- (1) Miller, J. A.; Kee, R. J.; Westbrook, C. K. *Annu. Rev. Phys. Chem.* **1990**, *41*, 345.
- (2) Miller, J. A.; Bowman, C. T. *Prog. Energy Combust. Sci.* **1989**, *15*, 287.
- (3) Medhurst, L. J.; Garland, N. L.; Nelson, H. H. *J. Phys. Chem.* **1993**, *97*, 12275.
- (4) Pilling, M. J.; Seakins, P. W. *Reaction Kinetics*; Oxford University Press: Oxford, 1995.
- (5) Goddard, W. A., III; Harding, L. B. *Ann. Rev. Phys. Chem.* **1978**, *29*, 363.
- (6) Walch, S. P. *J. Chem. Phys.* **1980**, *72*, 5679.
- (7) Robinson, G. W.; McCarty, M., Jr. *J. Am. Chem. Soc.* **1960**, *82*, 1859.
- (8) Goldfarb, T. D.; Pimentel, G. C. *J. Am. Chem. Soc.* **1960**, *82*, 1865.
- (9) Wasserman, E.; Barash, L.; Yager, W. A. *J. Am. Chem. Soc.* **1965**, *87*, 2075.
- (10) Milligan, D. E.; Jacox, M. E. *J. Chem. Phys.* **1966**, *44*, 2850.
- (11) Bondybey, V. E.; English, J. H. *J. Chem. Phys.* **1977**, *67*, 664.
- (12) DeKock, R. L.; Grev, R. S.; Schaeffer, H. F., III *J. Chem. Phys.* **1988**, *89*, 3016.
- (13) Wurfel, B. E.; Thoma, A.; Schlachta, R.; Bondybey, V. E. *Chem. Phys. Lett.* **1992**, *190*, 119.
- (14) Curtis, M. C.; Levick, A. P.; Sarre, P. J. *Laser Chem.* **1988**, *9*, 359. The LIF result of the CNN spin-orbit splitting is quite different than the matrix value [9 cm⁻¹] and is *A* = -26.5 cm⁻¹ in the gas phase.
- (15) Jacox, M. E. *Vibrational and Electronic Energy Levels of Polyatomic Transient Molecules*; American Institute of Physics: Woodbury, NY 11797-2999, 1994.
- (16) Bair, R. A. *Reaction of Methylidene with Molecular Nitrogen*; Argonne National Laboratory: 1985.
- (17) Ogilvie, J. F. *Can. J. Chem.* **1968**, *46*, 2472.
- (18) Leopold, D. G.; Murray, K. K.; Stevens Miller, A. E.; Lineberger, W. C. *J. Chem. Phys.* **1985**, *83*, 4849.
- (19) Ervin, K. M.; Lineberger, W. C. Negative Ion Photoelectron Spectroscopy. In *Gas Phase Ion Chemistry*; Adams, N. G., Babcock, L. M., Eds.; JAI Press: Greenwich, CT, 1992; Vol. 1, p 121.
- (20) Lee, J.; Grabowski, J. J. *Chem. Revs.* **1992**, *92*, 1611.
- (21) Kroeker, R. L.; Kass, S. R. *J. Am. Chem. Soc.* **1990**, *112*, 9024.
- (22) Arndt, F. In *Organic Synthesis Collective*; John Wiley & Sons: New York, 1943; Vol. II, p 165.
- (23) Neumark, D. M.; Lykke, K. R.; Andersen, T.; Lineberger, W. C. *Phys. Rev. A* **1985**, *32*, 1890. EA(O) = 11784.645 ± 0.006 cm⁻¹ or 1.461110 ± 0.000001 eV.
- (24) Siegel, M. W.; Celotta, R. J.; Hall, J. L.; Levine, J.; Bennett, R. A. *Phys. Rev.* **1972**, *A6*, 607.
- (25) Wang, T. C. L.; Ricca, T. L.; Marshall, A. G. *Anal. Chem.* **1986**, *58*, 2938.
- (26) Bartmess, J. E.; Georgiadis, R. M. *Vacuum* **1983**, *33*, 149.
- (27) Miller, K. J. *J. Am. Chem. Soc.* **1990**, *112*, 8533.
- (28) Van Doren, J. M.; Barlow, S. E.; DePuy, C. H.; Bierbaum, V. M. *Int. J. Mass Spectrom. Ion Processes* **1987**, *81*, 85.
- (29) Ervin, K. M.; Lineberger, W. C. *J. Phys. Chem.* **1991**, *95*, 1167. Photodetachment of HCC⁻ ion produces HCC (²Σ⁺) excited with one

quantum of the bend, ν_2 . Vibronic mixing of the ${}^2\Sigma^+$ and the low lying ${}^2\Pi$ electronic states of the ethynyl radical (HCC) by the CC–H bend is responsible for this breakdown of the Born–Oppenheimer approximation in ethynyl. The CNN system is different from HCC since the ground ${}^3\Sigma^-$ CNN state mixes with ${}^3\Pi$ CNN and $T_0({}^3\Pi$ CNN) is 23850 cm^{-1} in contrast to $T_0({}^2\Pi$ HCC) $\approx 3500\text{ cm}^{-1}$.

- (30) Ramsay, D. A.; Winnewisser, M. *Chem. Phys. Lett.* **1983**, *96*, 502.
 (31) Hougen, J. T.; Bunker, P. R.; Johns, J. W. C. *J. Mol. Spectrosc. C.* **1970**, *34*, 136.
 (32) Cooper, J.; Zare, R. N. *J. Chem. Phys.* **1968**, *48*, 942.
 (33) Gunion, R. F. *Ultraviolet Photoelectron Spectroscopy of Molecular Anions*. Ph.D. thesis, University of Colorado, 1995.
 (34) Frisch, M. J.; Trucks, G. W.; Schlegel, H. B.; Gill, P. M. W.; Johnson, B. G.; Robb, M. A.; Cheeseman, J. R.; Keith, T.; Petersson, G. A.; Montgomery, J. A.; Raghavachari, K.; Al-Laham, M. A.; Zakrzewski, V. G.; Ortiz, J. V.; Foresman, J. B.; Cioslowski, J.; Stefanov, B. B.; Nanayakkara, A.; Challacombe, M.; Peng, C. Y.; Ayala, P. Y.; Chen, W.; Wong, M. W.; Andres, J. L.; Replogle, E. S.; Gomperts, R.; Martin, R. L.; Fox, D. J.; Binkley, J. S.; Defrees, D. J.; Baker, J.; Stewart, J. P.; Head-Gordon, M.; Gonzalez, C.; Pople, J. A. *Gaussian 94*, Revision C.2 ed.; Gaussian, Inc.: Pittsburgh, PA, 1996.
 (35) Herzberg, G. H. *Molecular Spectra and Molecular Structure: Infrared and Raman Spectra of Polyatomic Molecules*; D. Van Nostrand: Princeton, New Jersey, 1945; Vol. II.
 (36) Davico, G. E.; Bierbaum, V. M.; DePuy, C. H.; Ellison, G. B.; Squires, R. R. *J. Am. Chem. Soc.* **1995**, *117*, 2590.
 (37) Pople, J. A.; Scott, A. P.; Wong, M. W.; Radom, L. *Is. J. Chem.* **1993**, *33*, 345.
 (38) Lias, S. G.; Bartmess, J. E.; Liebman, J. F.; Holmes, J. L.; Levin, R. D.; Mallard, W. G. *J. Phys. Chem. Ref. Data* **1988**, *17* (Suppl. 1), 1.
 (39) Berkowitz, J.; Ellison, G. B.; Gutman, D. *J. Phys. Chem.* **1994**, *98*, 2744.
 (40) DePuy, C. H.; Van Doren, J. M.; Gronert, S.; Kass, S. R.; Motell, E. L.; Ellison, G. B.; Bierbaum, V. M. *J. Org. Chem.* **1989**, *54*, 1846.
 (41) Laufer, A. H.; Okabe, H. *J. Am. Chem. Soc.* **1971**, *93*, 4137.
 (42) Benson, S. W. *Thermochemical Kinetics*, 2nd ed.; Wiley-Interscience: New York, 1976.
 (43) Gordon, M. S.; Kass, S. R. *J. Phys. Chem.* **1995**, *99*, 6548.
 (44) Gurvich, L. V.; Veyts, I. V.; Alcock, C. B.; Iorish, V. S. *Thermodynamic Properties of Individual Substances*, 4th ed.; Hemisphere: New York City, 1991; Vol. 2.
 (45) Clifford, E. P.; Wenthold, P. G.; Lineberger, W. C.; Petersson, G. A.; Ellison, G. B. *J. Phys. Chem.* **1997**, *101*, 4338.
 (46) Carter, E. A.; Goddard, W. A., III *J. Phys. Chem.* **1986**, *90*, 998.
 (47) Blush, J. A.; Clauberg, H.; Kohn, D. W.; Minsek, D. W.; Zhang, X.; Chen, P. *Acc. Chem. Res.* **1992**, *25*, 385.

- (48) Brzozowski, J.; Bunker, P.; Elander, N.; Erman, P. *Astrophysical Journal* **1976**, *207*, 414.
 (49) Huber, K. P.; Herzberg, G. *Constants of Diatomic Molecules*; Van Nostrand Reinhold: New York, 1979.
 (50) Helm, H.; Cosby, P. C.; Graff, M. M.; Moseley, J. T. *Phys. Rev. A* **1982**, *25*, 304.
 (51) Moore, C. E. *Atomic Energy Levels*; NSRDS-NBS 35; National Bureau of Standards: Washington, DC, 20402, 1971; Vol. 1.
 (52) Berkowitz, J.; Chupka, W. A.; Walter, T. A. *J. Chem. Phys.* **1969**, *50*, 1497.
 (53) Morely, G. P.; Lambert, I. R.; Ashfold, M. N. R.; Rosser, K. N.; Western, C. M. *J. Chem. Phys.* **1992**, *97*, 3157.
 (54) Berkowitz, J. Photoion-Pair Formation. In *VUV and Soft X-Ray Photoionization*; Becker, U., Shirley, D. A., Eds.; Plenum Press: New York, 1996; pp 263.
 (55) Bradforth, S. E.; Kim, E. H.; Arnold, D. W.; Neumark, D. M. *J. Chem. Phys.* **1993**, *98*, 800.
 (56) Huang, Y.; Barts, S. A.; Halpern, J. B. *J. Phys. Chem.* **1992**, *96*, 425.
 (57) Montgomery Jr., J. A.; Ochterski, J. W.; Petersson, G. A. *J. Chem. Phys.* **1994**, *101*, 5900.
 (58) Ochterski, J. W.; Petersson, G. A.; Montgomery Jr., J. A. *J. Chem. Phys.* **1996**, *104*, 2598.
 (59) Curtiss, L. A.; Raghavachari, K.; Trucks, G. W.; Pople, J. A. *J. Chem. Phys.* **1991**, *94*, 7221.
 (60) Hou, Z.; Bayes, K. D. *J. Phys. Chem.* **1993**, *97*, 1896.
 (61) Manaa, M. R.; Yarkony, D. R. *J. Chem. Phys.* **1991**, *95*, 1808.
 (62) Manaa, M. R.; Yarkony, D. R. *Chem. Phys. Lett.* **1992**, *188*, 352.
 (63) Walch, S. P. *Chem. Phys. Lett.* **1993**, *208*, 214.
 (64) Martin, J. M. L.; Taylor, P. R. *Chem. Phys. Lett.* **1993**, *209*, 143.
 (65) Seideman, T.; Walch, S. P. *J. Chem. Phys.* **1994**, *101*, 3656.
 (66) Seideman, T. *J. Chem. Phys.* **1994**, *101*, 3662.
 (67) Berman, M. R.; Lin, M. C. *J. Phys. Chem.* **1983**, *87*, 3933.
 (68) Thomson, C. *J. Chem. Phys.* **1973**, *58*, 841.
 (69) Murray, C. W.; Laming, G. J.; Handy, N. C.; Amos, R. D. *J. Phys. Chem.* **1993**, *97*, 1868.
 (70) Suter, H. U.; Huang, M.-B.; Engels, B. *J. Chem. Phys.* **1994**, *101*, 7686.
 (71) Chase, M. W., Jr.; Davies, C. A.; Downey, J. R., Jr.; Frurip, D. J.; McDonald, R. A.; Syverud, A. N. *J. Phys. Chem. Ref. Data* **1985**, *14* (Suppl. 1), 1.
 (72) Ervin, K. M.; Gronert, S.; Barlow, S. E.; Gilles, M. K.; Harrison, A. G.; Bierbaum, V. M.; DePuy, C. H.; Lineberger, W. C.; Ellison, G. B. *J. Am. Chem. Soc.* **1990**, *112*, 5750.